

ULTRA-HIGH DENSITY ELECTRON BEAMS FOR BEAM RADIATION AND BEAM PLASMA INTERACTION*

S. G. Anderson, W.J. Brown, D. J. Gibson, F. V. Hartemann, J. S. Jacob, A. M. Tremaine
LLNL, Livermore, CA 94550, USA

J. K. Lim, P. Frigola, P. Musumeci, J. B. Rosenzweig, G. Travish
UCLA, Los Angeles, CA 90095, USA

Abstract

Current and future applications of high brightness electron beams, which include advanced accelerators such as the plasma wake-field accelerator (PWFA) and beam-radiation interactions such as inverse-Compton scattering (ICS), require both transverse and longitudinal beam sizes on the order of tens of microns. Ultra-high density beams may be produced at moderate energy (50 MeV) by compression and subsequent strong focusing of low emittance, photoinjector sources. We describe the implementation of this method used at the PLEIADES ICS x-ray source in which the photoinjector-generated beam has been compressed to 300 fsec duration using the velocity bunching technique and focused to 20 μm rms size using an extremely high gradient, permanent magnet quadrupole (PMQ) focusing system.

INTRODUCTION

The performance of many high brightness electron beam applications depends on the production of very dense beams. Examples of these applications include the driving of a PWFA [1] and providing an electron beam for an ICS x-ray source [2]. The need for shorter bunch lengths, σ_z , and lower transverse emittances, $\varepsilon_{x,y}$, has driven work on photoinjector optimization, bunch compression systems, and the development of future electron beam sources. In addition, proportional scaling of the dimensions of the beam focal system must be considered to produce ultra-dense beams.

Examine in turn the two examples of PWFAs and ICS sources. In a PWFA, the maximum accelerating field, the “wave-breaking” field, achievable in a relativistic plasma wave is $E_{WB} = m_e c^2 k_p / e$, where k_p is the plasma wave number. If the driving beam is short ($k_p \sigma_z < 1$), then the wake is efficiently excited and the electric field of the plasma wave scales as $E \propto k_p^2 N_b$. Therefore, larger accelerating fields are obtained by operating a larger k_p , and shorter σ_z . The use of large plasma wavenumbers effects the transverse forces as well, as can be seen from the matched β -function associated with the plasma’s ion-

derived focusing,

$$\beta_{eq} = \sqrt{2\gamma} k_p^{-1}. \quad (1)$$

For low energy experiments, β_{eq} can be extremely short, and has already been in the range of several mm [3].

In the case of ICS sources, the rate of x-ray photons production, dN_x/dt , depends on the intensities of the overlapping electron and laser beams, and the duration of the interaction. Assuming a 180° interaction geometry, Gaussian laser and electron beam profiles, and that the beam dimensions do not change significantly during the interaction, the number of x-rays produces is

$$N_x = \frac{N_e N_L \sigma_T}{2\pi(\sigma_e^2 + \sigma_L^2)}, \quad (2)$$

where N_e and N_L are the number of input electrons and photons, respectively, σ_e and σ_L are the beam rms sizes, and σ_T is the total Thomson cross section. The x-ray source brightness, often a more important figure of merit for applications, is given by

$$\mathcal{B}_x = \frac{N_x}{(2\pi)^{5/2} \sigma_x^2 \sigma_{x'}^2 \sigma_\tau (0.1\% \text{BW})}. \quad (3)$$

Since the source size, σ_x , divergence, $\sigma_{x'}$ and duration, σ_τ are all strongly coupled to the electron bunch phase space, it is clear that the electron beam brightness, in addition to density, should be maximized for x-ray production.

Magnetic compression schemes have proven successful in producing sub-ps beams generated by photoinjectors. The effect of the compression process on the transverse phase space, however has been determined to be damaging, both at low energies due to space-charge forces [4], and at higher energies due to coherent synchrotron radiation [5]. This observed emittance growth runs counter to the goal of increasing the beam brightness that motivates the use of compression to begin with. The “velocity bunching” scheme, proposed by Serafini and Ferrario [6], may preserve the transverse phase space quality, while compressing the beam to sub-ps bunch length [7]. This scheme, as opposed to the path-length dependence of magnetic compression systems, is an extension of the commonly employed technique of RF rectilinear compression. As design trajectory bending is not needed in this system, one may avoid the phase space degrading effects observed in magnetic compression experiments on photoinjector-derived beams.

* This work was performed under the auspices of the U.S. Department of Energy by the University of California, Lawrence Livermore National Laboratory under contract No. W-7405-Eng-48, and by the University of California, Los Angeles under contract numbers DE-FG-98ER45693 and DE-FG03-92ER40693

In order to create minimum β -functions small enough for modern high-brightness electron beam applications, one must look into the use of much shorter focal length lenses. This is motivated by the need to avoid chromatic aberrations due to energy spread, and emittance growth due to residual space-charge effects in the beam if it is expanded for final focusing. Permanent magnet-based quadrupoles (PMQs) can access high-field gradients, and have been under intensive study recently [8]. They offer the advantages of simplicity and being relatively inexpensive when compared to alternatives such as superconducting systems, or plasma lenses.

In this paper we describe the implementation of both the velocity bunching technique [9] and a PMQ based final focus system [10] at the PLEIADES ICS X-ray source [11], a collaboration between LLNL and UCLA. Both of these measures have improved the performance of the X-ray source.

VELOCITY BUNCHING

In the velocity bunching method, an energy/phase correlation is imparted to the electron beam and removed smoothly, through phase slippage and acceleration, inside of an rf linac section. In this method the beam is rotated through one quarter of a phase space oscillation. The electron trajectories in the sinusoidal longitudinal electric field component of the RF wave in a traveling wave structure can be tracked and plotted in (ϕ, γ) phase space using the electron equations of motion; $\frac{d\gamma}{dz} = -\alpha k \sin \phi$, and $\frac{d\phi}{dz} = k \left[1 - \frac{\gamma}{\sqrt{\gamma^2 - 1}} \right]$.

Particles injected at or near $\phi_0 = 0$ will begin to slip into an accelerating phase. As the particles accelerate to ultra-relativistic velocity, the phase slippage slows, and is eventually arrested. In terms of the particle's initial phase space coordinates (ϕ_0, γ_0) , the asymptotic value of the slipping phase is $\phi_\infty \cong \cos^{-1} \left[\cos \phi_0 - \frac{1}{2\alpha\gamma_0} \right]$.

The phase space rotation occurs as a result of the varying orientation of the phase contour lines. If two particles are injected at $\phi_0 = 0$ with a difference in phase but no spread in energy, such that they align parallel to a phase contour, then they will remain parallel to that contour as they slip in phase and accelerate. As the particles approach ϕ_∞ , their orientation becomes nearly parallel to the γ axis, having rotated by nearly 90 degrees.

The PLEIADES photoinjector and linac consist of a 1.6 cell photo-cathode RF gun followed by four SLAC style 2.5 meter, S-band traveling wave sections. While the linac is capable of producing 100 MeV electrons, it is typically run using only the first two or three sections for X-ray production, resulting in beam energy between 20 and 70 MeV. Velocity bunching has been performed with this system using the travelling wave section immediately following the gun to compress the beam, while the remaining sections were used to accelerate the beam on-crest, thereby reducing the relative energy spread.

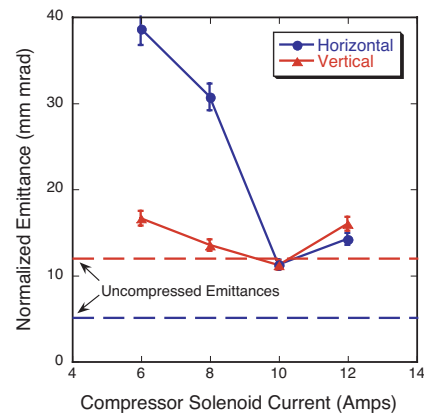


Figure 1: Measured horizontal and vertical normalized emittances of the 300 fsec beam versus the compressor solenoid strength.

The longitudinal dynamics in the experiment agreed well with those found in simulations. A 250 pC bunch was compressed from an initial duration of 3 ps (rms) to a final length of 300 fs. The bunch length was measured using a coherent transition radiation based interferometer [12]. The energy spread of the compressed beam, accelerated to 50 MeV, was 0.5%. Again, in agreement with simulations, and higher than the nominal uncompressed value of 0.2%.

Transversely, the increasing space-charge forces resulting from the increasing beam current in the compressor must be matched with external focusing to minimize space-charge induced emittance growth. This external focusing was provided in the experiment by a solenoid field along the length of the compressing rf section. The emittance of the compressed electron beam was measured using the quadrupole scanning method for various settings of the solenoid field strength. The results of those measurements are shown in Fig. 1. As expected, the emittance shows a very strong dependence on the compressor focusing, growing by a factor of 3 in $\varepsilon_{n,x}$ with a 20% change in solenoid current. A minimum of 11 mm mrad in both emittances was found to occur at the 10 A solenoid setting in this scan.

The velocity compressed beam was used in conjunction with a Ti:Sapphire-based, 500 mJ, 50 fs (FWHM), 800 nm laser pulse for ICS x-ray generation. The compressed beam was measured to be roughly 50% larger in x and y than the uncompressed beam at final focus. This increase is due to both the increased energy spread of the compressed bunch, and emittance growth. A comparison of the resulting x-ray pulses is shown in Fig. 2. While the increased final focus spot size reduces the total number of scattered photons, the *brightness* of the 300 fsec bunch is increased by 70% from that of the x-rays produced without velocity bunching.

PMQ FOCUSING

PMQs were chosen to deliver the extremely high magnetic field gradients desirable in the PLEIADES final fo-

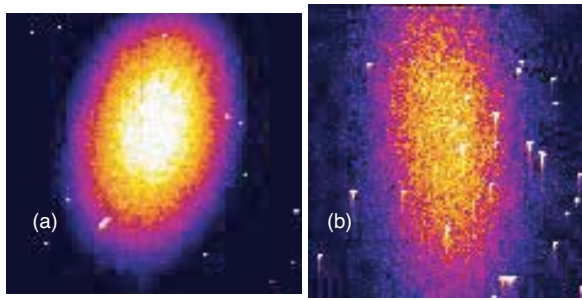


Figure 2: Single shot, false-color X-ray beam images measured by a CCD for the (a) uncompressed and (b) compressed electron beams.

cus system. A 16-segment Halbach configuration [13] was simulated with the 3D magnetostatic code, RADIA, using PM material (NdFeB) with a 1.22 T remanent field, 5 mm inner diameter, and a 15 mm outer diameter. The field gradient produced in the simulation was $B' = 573$ T/m, slightly lower than the theoretical prediction for this design due mainly to three-dimensional (edge) effects. The quadrupole length was chosen based on the theoretical and simulation predictions so that the focusing phase advance in a single lens is less than one-half for a 70 MeV beam ($k_q l_q \leq 0.5$).

A series of RADIA simulations were performed in order to evaluate the performance of the magnet design in the presence of fabrication and assembly errors. The following results were obtained: (1) a magnetization easy-axis angular orientation error is allowable up to 2% before a notable change develops between the magnetic center and the mechanical center; (2) the wedge shape error (the wedge angle) is limited and allowed up to again 2%; and finally (3) bore radius variations of ± 0.05 mm from the nominal 2.5 mm radius produced the field gradient variation of 3% from the ideal B' . These results were then used to apply magnetic field errors in ELEGANT simulations of the final focus using input beam parameters typical of the PLEIADES experiment. The most significant source of emittance growth was found to be rotation (skew) error between successive magnets. A 10 mrad rotation error was found to result in a doubling of the emittance of the beam at focus, with a corresponding increase in spot size.

The fabrication of PMQs with the required precision proved to be a technically challenging task. Nevertheless, a simplified procedure may be given as follows: a long trapezoidal wedge which is pre-magnetized to a $B_r = 1.22$ T is machined to a specified design shape from a larger magnet block through wire electrical discharge machining. The 16 magnetized wedges are then coupled together into an equally long aluminum keeper tube. A thin layer of cohesion material is applied, strongly joining neighboring magnets. The tube keeper and a bonding glue together ensure structural stability of the PMQ under extreme magnetic repulsions. The long assembly is then cut into six identical

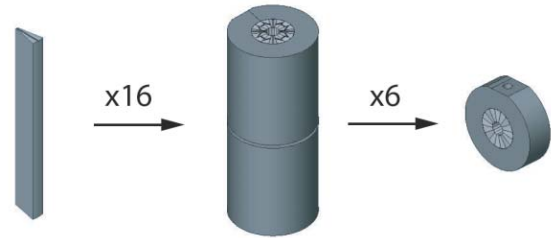


Figure 3: An illustration of the PMQ manufacturing process showing an individual wedge, the assembled 16 wedge rod, and a single PMQ cut from the rod.



Figure 4: An assembled PMQ.

PMQs, with mechanical length of 10 cm, to ensure consistent performance between all PMQs. In particular, construction of a single, long magnet assembly assured that the relative azimuthal (roll) errors of individual units may be essentially eliminated. Finally, the inner diameter of bore is slowly ground to the specified value of 5 mm with a diamond cutter. An illustration which schematically summarizes the PMQ fabrication procedure is shown in Fig. 3. One of the produced magnets is shown in Fig. 4.

Measurements of the individual magnets were performed using both a Hall probe and the pulsed wire technique [14]. These measurements were found to agree well with RADIA simulations, as Fig. 5 demonstrates. The Hall probe measured field gradient was $B' = 560$ T/m in the center of the PMQ bore region, while the pulsed wire measurements verified the co-location of the mechanical and magnetic centers to within $25 \mu\text{m}$.

For the final focus system, a simplified thin lens triplet design was analyzed. Assuming a symmetric beam waist at both the focus and the input to the triplet, and given a minimum achievable lens focal length f_{min} , it can be shown that optimal focusing is found in an asymmetric design in which the lens focal lengths are $2f_{min}$, $-f_{min}$, f_{min} . Based on this analysis, and verification of the (F-DD-FF) configuration using TRACE3D simulations, the PMQ “mover system” was designed to independently position (thereby providing tunability) 3 separate lenses, the first being a single PMQ, and the following two consisting

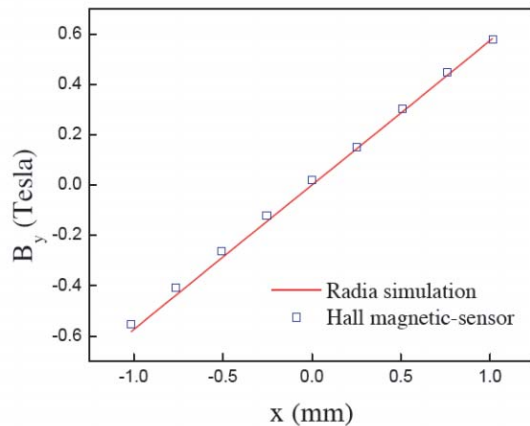


Figure 5: A comparison of PMQ field profile measurements using a Hall probe to RADIA simulation results.

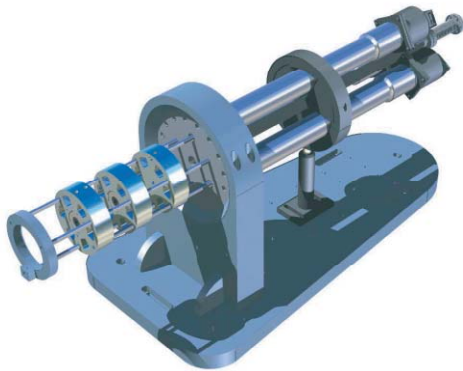


Figure 6: A rendered CAD drawing of the final-focus assembly.

of two concatenated magnets.

The PMQ mover assembly, illustrated in Fig. 6, was built and later measured to position the magnets with a level of precision as described above, and installed in the PLEIADES interaction beamline. The assembly consists of a rail system which maintains the alignment of each magnet, and a set of push-rods connected to stepper motor driven vacuum linear motion feedthroughs.

The PMQ system has successfully focused beams from 50 to 90 MeV, demonstrating the tunability of this system. The beam spot size at the focus was measured using optical transition radiation (OTR) generated as the electrons impact a polished metal surface. Figure 7 show a CCD image of the final focus produced using a 200 pC, 70 MeV beam. The spot size, 20 μm , is a significant improvement over that obtained with the previously employed electromagnet based final focus system. The final focus tunability has been used to produced ICS x-rays over the range from 40 to 140 keV.

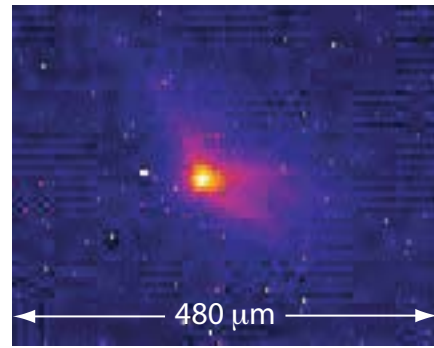


Figure 7: False color CCD image of the PMQ focused electron beam. The RMS beam size is 20 μm in both x and y .

REFERENCES

- [1] P. Chen, J.M. Dawson, R.W. Huff, and T. Katsouleas, Phys. Rev. Lett. **54**, 693 (1985); P. Chen, J.M. Dawson, R.W. Huff, and T. Katsouleas, Phys. Rev. Lett. **55**, 1537 (1985); J.B. Rosenzweig, B. Breizman, T. Katsouleas, and J.J. Su, Phys. Rev. A **44**, R6189 (1991).
- [2] R.W. Schoenlein *et al.*, Science **274**, 236 (1996); I.V. Pogorelsky *et al.*, Phys. Rev. ST Accel. Beams **3**, 090702 (2000).
- [3] N. Barov *et al.*, Phys. Rev. ST Accel. Beams **3**, 011301 (2000).
- [4] H. Braun *et al.*, Phys. Rev. Lett. **84**, 658 (2000); S.G. Anderson, J.B. Rosenzweig, P. Musumeci, and M.C. Thompson, Phys. Rev. Lett. **91**, 074803 (2003).
- [5] J.S. Nodvick and D.S. Saxon, Phys. Rev. **96**, 180 (1954); K. Ishi *et al.*, Phys. Rev. A **43**, 5597 (1991); S. Heifets, G. Stupakov, and S. Krinsky, Phys. Rev. ST Accel. Beams **5**, 064401 (2002).
- [6] L. Serafini and M. Ferrario, in Physics of, and Science with, the X-ray Free-Electron Laser, AIP Conf. Proc. No. 581 (2001).
- [7] X.J. Wang, X. Qiu, and I. Ben-Zvi, Phys. Rev. E **54**, R3121 (1996); P. Piot, L. Carr, W.S. Graves, and H. Loos, Phys. Rev. ST Accel. Beams **6**, 033503, (2003).
- [8] W. Lou *et al.*, in Proceedings of the 1997 Particle Accelerator Conference, 3236, (1998); J.T. Volk *et al.*, in Proceedings of the 2001 Particle Accelerator Conference, 217, (2001).
- [9] S.G. Anderson *et al.*, Phys. Rev. ST Accel. Beams **8**, 014401 (2005).
- [10] J.K. Lim *et al.*, Submitted to Phys. Rev. ST Accel. Beams (2005).
- [11] D.J. Gibson *et al.*, Physics of Plasmas **11**, 2857, (2004).
- [12] A. Murokh *et al.*, Nucl. Instrum. Methods Phys. Res., Sect. A **410**, 452 (1998).
- [13] K. Halbach, Nuclear Instruments and Methods **169**, 1 (1980); K. Halbach, Nuclear Instruments and Methods **198**, 213 (1982).
- [14] R. Warren, Nucl. Instrum. Methods Phys. Res., Sect. A **272**, 257 (1988).